

Evolution of Stellar Collision Products in Globular Clusters – I. Head-on Collisions.

Alison Sills

Department of Astronomy, Yale University, P.O. Box 208101, New Haven, CT, 06520-8101,
USA

James C. Lombardi¹

Center for Radiophysics and Space Research, Cornell University, Ithaca, NY 14853, USA

Charles D. Bailyn, Pierre Demarque

Department of Astronomy, Yale University, P.O. Box 208101, New Haven, CT, 06520-8101,
USA

Frederic A. Rasio

Department of Physics, MIT 6-201, Cambridge, MA 02139, USA

Stuart L. Shapiro²

Department of Physics, University of Illinois at Urbana-Champaign, 1110 West Green
Street, Urbana, IL 61801, USA

Received _____; accepted _____

¹also Department of Astronomy, Cornell University

²also Department of Astronomy and National Center for Supercomputing Applications,
University of Illinois at Urbana-Champaign

ABSTRACT

We explore the evolution of collisionally merged stars in the blue straggler region of the HR diagram. The starting models for our stellar evolution calculations are the results of the smoothed particle hydrodynamics (SPH) simulations of parabolic collisions between main sequence stars performed by Lombardi, Rasio and Shapiro (1996). Since SPH and stellar evolution codes employ different and often contradictory approximations, it is necessary to treat the evolution of these products carefully. The mixture and disparity of the relevant timescales (hydrodynamic, thermal relaxation and nuclear burning) and of the important physical assumptions between the codes makes the combined analysis of the problem challenging, especially during the initial thermal relaxation of the star. In particular, the treatment of convection is important, and semiconvection must be modeled in some detail.

The products of seven head-on collisions are evolved through their initial thermal relaxation, and then through the main sequence phase to the base of the giant branch. Their evolutionary tracks are presented. In contrast to the assumptions in previous work, these collision products do not develop substantial convective regions during their thermal relaxation, and therefore are not mixed significantly after the collision.

Subject headings: stellar collisions – stellar evolution – blue stragglers – globular clusters – hydrodynamics

1. Introduction

Blue stragglers are main sequence stars which are more massive than the main sequence turnoff stars in clusters. Since massive stars evolve more quickly than low mass stars, blue stragglers must have been born (or reborn) on the main sequence more recently than the majority of the stars in the cluster. Numerous formation mechanisms have been proposed (for a recent review, see Stryker 1993). The current observations suggest that stellar collisions could be a viable mechanism for some blue stragglers (Bailyn 1995).

In most environments, collisions between stars are very rare events. However, the cores of some globular clusters are dense enough that collisions between single stars are expected to happen at dynamically significant rates (Hills & Day 1976). Also, binary star systems have a much larger collisional cross-section than single stars and can enhance the number of stellar collisions (Leonard 1989, Sigurdsson & Phinney 1993).

It is important to include the effects of physical collisions between stars when studying the dynamics and overall evolution of globular clusters. These collisions produce stars which are more massive than most of the stars in clusters. The relative proportions of stars of different masses affect the rate at which various dynamical processes occur, such as core collapse and mass segregation (Elson, Hut & Inagaki 1987). The exchange of energy between the cluster kinetic energy and the collisional energy can also affect dynamical processes. Therefore, it is important to determine how many massive stars are created by collisions. Stellar collisions are also important tracers of the dynamical state of globular clusters. The collision rates and participants are determined by global cluster properties such as density, velocity dispersion, mass function and mass segregation. Therefore, by studying the products of stellar collisions, we will be able to probe the dynamics, both past and present, of globular clusters.

To fully study the consequences of stellar collisions in globular clusters, many different

lines of investigation need to be combined. We need to know how many collisions happen in a particular cluster, as well as what kinds of collisions occur, between which kinds of stars, and with what frequency. These questions can be answered with multi-mass King-Mitchie models (eg., Davies & Benz 1995) which give the density and velocity dispersion of the clusters. Two- and three-body scattering experiments (eg. McMillan & Hut 1996, Davies, Benz & Hills 1994) can determine the probabilities for different kinds of collision products to be produced.

In addition to determining the global collision properties of the cluster, we need to consider individual collisions. SPH calculations of stellar collisions relevant to stars in globular clusters (eg. Benz & Hills 1987, Lombardi *et al.* 1995, 1996 (hereafter LRS), Sandquist *et al.* 1996) can provide a detailed description of the structure and composition of the collision product. Stellar evolution calculations can then follow the evolution of the collision product to determine its track in a color-magnitude diagram, whether or not it has surface abundance anomalies, and other observable properties (e.g. rotation rate or pulsation period).

Previous evolution studies (Bailyn & Pinsonneault 1995, Sills *et al.* 1995, Ouellette & Pritchett 1996, Sandquist *et al.* 1996) used only a portion of the SPH results to model collision products. These groups imposed the chemical profile, but not the structure, of a collision product on an otherwise normal stellar model, and compared the evolution of these stars to that of fully mixed models. The results of these studies are inconsistent. Bailyn & Pinsonneault (1995) and Sills *et al.* 1995 demonstrated that the blue stragglers in 47 Tuc and the brightest blue stragglers in NGC 6397 could be explained only by fully mixed models. However, the SPH simulations show that the collision product is not thoroughly mixed by the collision. Therefore, the blue stragglers would have to be mixed by some process which occurs after the collision, not during it.

Leonard & Livio (1995) proposed such a mechanism. They suggested that the collision products will contain a large amount of thermal energy deposited by the collision, and consequently will swell up into something resembling a pre-main sequence star with a large convective envelope. Under this assumption, blue stragglers will be largely or fully mixed due to convection when they arrive on the main sequence despite the fact that the collision itself does not result in a significant amount of mixing. This scenario is based on the speculation that stellar collision products contain enough thermal energy to become pre-main sequence stars. It was not clear whether this situation would actually occur or not. Sandquist *et al.* (1996) modeled the Leonard & Livio scenario by adding enough energy to their initial stellar models that the stars were on the Hayashi track, and then began their evolutionary runs. As a result, their stars developed large surface convective zones, and also small, short-lived convective cores. A significant fraction of the more massive collision products were mixed as a result of the convection.

In this paper, we present a set of evolution calculations based on more rigorous initial conditions than used in the previous studies. Instead of imposing the collisional chemical composition profile on an otherwise normal stellar model, we use all the stellar structure information from the SPH results in the starting models for our evolution calculations. We do not add energy to our models since we do not want to make any assumptions about where in the HR diagram the collision models should reside. In particular, we wish to investigate the apparent discrepancy between the negligible amount of mixing which is caused by the collision itself, and the substantial amount of mixing which seems necessary to explain at least some blue stragglers in some clusters. We concentrate on the head-on collisions in this paper. Future work will incorporate the results from non-head-on collisions, and we will use population synthesis techniques to compare our theoretical predictions with observations.

In section 2 we describe the different tools used in this work. In section 3 we discuss

the details of converting an SPH collision product to a valid evolutionary starting model, and in section 4 we present the results of the evolutionary calculations. In section 5 we discuss the implications of these models to the origins of blue stragglers, and detail future work to be done.

2. Numerical Methods

The following section briefly describes the SPH and stellar evolution codes used in this study. We highlight the differences in underlying physical assumptions, which must be dealt with carefully in using the output of the SPH code as input for stellar evolution calculations.

2.1. The Smoothed Particle Hydrodynamics Code

SPH is a Lagrangian method and therefore ideally suited to follow chemical mixing during the stellar collision. LRS used a modified version of the code developed by Rasio (1991) specifically for the study of stellar interactions. Fluid elements are represented by SPH “particles”, and associated with each particle is its position \mathbf{r} , velocity \mathbf{v} , mass m , entropy s and a purely numerical “smoothing length” h specifying the local spatial resolution. Local quantities are calculated by weighted sums over nearby particles. The LRS collision simulations solve the equations of motion of a large number (typically 3×10^4) of particles, interacting by both gravitational and hydrodynamic forces, and yield accurate structural and chemical composition profiles for the merger remnant.

LRS performed SPH calculations of twenty-three parabolic collisions with various mass combinations and impact parameters. The parent stars were main sequence stars appropriate for globular clusters, with chemical composition profiles based on evolutionary

models evolved to 15 Gyr. The $M = 0.8M_{\odot}$ star was modeled as an $n = 3$ polytrope, the $M = 0.4M_{\odot}$ star was modeled as an $n = 1.5$ polytrope, and the $M = 0.6M_{\odot}$ star was a composite polytrope with an $n = 3$ core and an $n = 1.5$ envelope. In all cases, the fluid was treated as an ideal gas with adiabatic index $\Gamma_1 = 5/3$. The parent models and final results are described in detail in LRS.

SPH codes, by definition, are hydrodynamic and can deal with 3-dimensional fluids which are far from hydrostatic equilibrium. They follow the system over dynamical timescales, which are typically on the order of an hour for collisions involving main sequence stars in globular clusters. The adopted SPH code includes the effects of shocks, but is adiabatic and otherwise neglects all radiative and heat transport between particles, which is not significant on dynamical timescales. Therefore, convective energy transport is not modeled, but the mixing effects of convective fluid motions occurring on a dynamical timescale are included.

2.2. The Stellar Evolution Code

We used the Yale Rotating Evolution Code (YREC) in its non-rotating mode for our stellar evolution calculations. The code solves the equations of stellar structure in one dimension using the Henyey technique. A detailed description of the physics included in the code can be found in Guenther *et al.* (1992). We have since updated the opacities to include OPAL opacities for $\log T \geq 4.00$ (Iglesias & Rogers 1996) and Alexander low temperature opacities for $\log T \leq 4.00$ (Alexander & Ferguson 1994) We chose a mixing length of 1.9 pressure scale heights, the value which gives a standard solar model using this code. For the head-on collisions, the assumption of non-rotation is justified, since the initial conditions have zero angular momentum. However, the products of grazing collisions are rotating rapidly and consequently aspherical. In future work involving non-head-on

collisional remnants, the structural and mixing effects of rotation will be included.

YREC assumes that the star is in hydrostatic equilibrium, and uses a 1-dimensional treatment where the star is modeled as a series of concentric shells. One of the main concerns is to follow energy transport closely. The timescales for evolution codes range from thermal ($\sim 10^6$ years) to nuclear ($\sim 10^9$ years) timescales. All of these assumptions are drastically different from those used by the SPH code.

3. Preparing the Collision Models for Evolution

The different assumptions about the important physics, the timescales and geometry treated by SPH and stellar evolution codes create difficulties in converting the SPH results into an acceptable starting model for use in YREC. This section describes our approach for dealing with each of these assumptions. Figures 1, 2 and 3 show the structure of three collision remnants immediately after their conversion to YREC format.

3.1. Spherical Symmetry

The first step is to turn the 3-dimensional particle data from SPH into 1-dimensional radial profiles. The SPH particles which remained gravitationally bound to the collision product were divided into 32-45 spherical shells. The entropy and composition of the SPH particles in each shell were averaged to give a value for that shell. Since YREC is more accurate with more shells, the number of shells was increased to 1500 by interpolating each quantity using a cubic spline. A visual comparison of the resulting entropy and composition profiles with the profiles of LRS shows that no significant spurious oscillations were introduced by this interpolation technique. To ensure smoothness in the derivatives of the profiles, we interpolated off of carefully chosen mass shells not evenly spaced in mass

fraction; however, the evolutionary tracks are virtually unaffected by the particular choice of mass shells used.

Since YREC solves the equations of stellar evolution in one dimension, all stars are assumed to be spherically symmetric. This constraint poses two problems. The first is that the head-on collision products are not spherically symmetric in their chemical composition. We therefore took the average of all particles in given shells. It can be shown (appendix A) that this is a plausible approximation. The second problem caused by the requirement of spherical symmetry is for non-head on collisions (the general case) the collision products are rotating rapidly. However, the products of head-on collisions are not rotating, so we treat only spherically symmetric models in this paper. As can be seen in figure 8 of LRS, this assumption of spherically symmetric structure for head-on collisions is quite realistic.

3.2. Hydrostatic Equilibrium

Starting with the entropy and composition profiles provided by the SPH simulations of LRS, we calculated the pressure and density profiles of each collision product by integrating the equation of hydrostatic balance and imposing the boundary condition $P(M) = 0$. This procedure ensures that the initial evolutionary models are in hydrostatic equilibrium. The pressure and density profiles were not taken directly from the SPH results since these profiles are not accurate enough to guarantee hydrostatic equilibrium at the level of precision needed for YREC.

Since, at the termination of the SPH simulation, the outermost 2–4% of the gravitationally bound fluid is still far from dynamical equilibrium, we do not use the SPH entropy profile in this region but rather use the cubic spline to extrapolate from the interior so that entropy increases with mass fraction throughout the star. We tested a number of

schemes for approximating the profiles in the outer few percent and found that the tracks converged after a few evolutionary timesteps: the stellar interior is vastly more important in determining long-lived global characteristics.

These starting models have therefore been constructed to be in precise hydrodynamical equilibrium, although they are typically far from thermal equilibrium. The initial density and pressure profiles input to YREC differ somewhat from the final SPH profiles of LRS for two reasons. First, the averaging over nearest neighbors in the SPH scheme makes the central density and pressure smaller than they should be for hydrostatic balance (these errors in the SPH scheme vanish in the limit of perfect spatial resolution). Secondly, the SPH density and pressure depend on when the collision simulation is terminated, since they continually change as fluid falls back to the stellar surface. Note, however, that the entropy profile is virtually unaffected by the hydrodynamics of the outermost region and is therefore appropriate for determining the profiles of the collision product in complete hydrostatic equilibrium.

3.3. Equation of State

We used the equation of state and the previously determined profiles of pressure and density to calculate the temperature profile of the collision product. While SPH assumes a fully ionized ideal gas equation of state, YREC uses a much more sophisticated equation of state including radiation pressure, electron degeneracy and the effects of partial ionization. For the stars we are considering, the ideal gas equation of state is a very good approximation, with the only significant correction being radiation pressure. We used the YREC implementation of the Saha equation to determine the number of free electrons per nucleon in each shell for temperatures less than $\log T = 6.3$, and assumed that the gas was fully ionized for hotter regions.

3.4. Energy Transport

Since the SPH code did not include energy transport, it gives no direct information about luminosity. We used the equation of radiative transport

$$\frac{dT}{dm} = \frac{-3}{64\pi^2ac} \frac{\kappa L(m)}{r^4 T^3} \quad (1)$$

to give us $L(m)$, the luminosity for each shell. Here T is the temperature and r is the radius of that shell. The opacity κ includes both radiative and conductive opacities. Equation (1) is a good approximation at $t = 0$ since none of the initial models contain convective regions. The unusual luminosity profiles obtained reflect the strongly non-equilibrium distribution of internal energy caused by the collision and constitute one of the major differences from more straightforward approximations (see figures 1, 2 and 3). For example, the luminosity in case G is initially negative near $m/M \approx 0.25$, which is a direct consequence of $dT/dm > 0$ in this region.

4. Evolution of the Collision Products

Here we discuss the results of evolving the seven head-on LRS collision products. A summary of the collision products is given in table 1. We emphasize the results of three particular collisions which demonstrate important features of the evolution calculations: case A ($0.8M_{\odot} + 0.8M_{\odot}$), case G ($0.8M_{\odot} + 0.4M_{\odot}$) and case J ($0.6M_{\odot} + 0.6M_{\odot}$). Case A was chosen to represent the most massive collision product. We also chose to discuss two collision products (cases G and J) with similar masses but very different collisional histories to demonstrate that collisional history is at least as important as final mass in determining the evolutionary track of the collision product.

4.1. Procedure

After converting each of the SPH models into a starting model for YREC, the stars were evolved with timesteps of 1×10^2 to 5×10^2 years (about 10^{-4} of a thermal timescale) through their initial thermal relaxation phase. This value was chosen to ensure that the evolutionary timestep was shorter than the local thermal timescale for most of the star. When the star reached the main sequence, the short timestep constraint was lifted, and timesteps were chosen automatically to maximize the efficiency of the computing. The evolution was stopped when the star reached the giant branch.

For comparison, we also evolved normal stars with masses similar to the collision products. To create the starting models for these stars, we calculated fully convective polytropes ($n = 1.5$) with the same initial composition as the collision products ($Y = 0.25, Z = 0.001$). We then evolved these models from the pre-main sequence to the main sequence and beyond to the giant branch.

To determine the maximum effect mixing could have on the evolution, we also evolved fully mixed collision products, with helium abundances higher than a normal globular cluster star. The chemical composition of the SPH model was averaged over the entire star, keeping the total helium mass the same but spreading the hydrogen and helium evenly throughout the star. These stars were also evolved from $n = 1.5$ polytropes.

4.2. Convection and Semiconvection

Convection is a hydrodynamical process, since it involves the motion of fluid elements. It is also a thermal process, since convection transports energy. Since the SPH code does not model energy transport, and the evolution code does not model dynamical processes, both codes have to treat convection as an approximation. The convective turnover timescale

for stars like the sun is typically on the order of a month. This timescale is between the hour-long dynamical timescale followed by the SPH code, and the century-long timescale which is the shortest numerically stable timestep in YREC. Therefore, convection is the most important process which spans all timesteps and both codes, and must be treated with particular care.

YREC, in its original form, uses the Schwarzschild criterion for stability,

$$\nabla_{rad} < \nabla_{ad} \quad (2)$$

where $\nabla_{rad} = \left(\frac{d \ln T}{d \ln P}\right)_{rad}$ is the radiative temperature gradient and ∇_{ad} is the adiabatic temperature gradient, without regard for the presence of composition gradients. However, a gradient in the mean molecular weight μ within the star can stabilize the fluid against convection, and so it may be necessary to use the more general Ledoux criterion,

$$\nabla_{rad} < \nabla_L \equiv \nabla_{ad} + \frac{\varphi}{\delta} \nabla_{\mu} \quad (3)$$

where $\nabla_{\mu} = \frac{d \ln \mu}{d \ln P}$ is the mean molecular weight gradient, and $\varphi = \left(\frac{d \ln \rho}{d \ln \mu}\right)_{P,T}$ and $\delta = -\left(\frac{d \ln \rho}{d \ln T}\right)_{P,\mu}$ are quantities which depend on the equation of state. It is possible that a particular shell is stable against convection according to the Ledoux criterion but unstable according to the Schwarzschild criterion. This situation is called semiconvection. Fluid elements in these regions are vibrationally unstable and oscillate slowly about their initial position with increasing amplitude (see e.g. Kippenhahn & Weigert 1994)

Semiconvective regions mix on a thermal timescale until the mean molecular weight gradient becomes small enough that the region is stable against semiconvection. Using only the Schwarzschild criterion is an acceptable approximation for most evolution calculations, since the evolution timesteps are longer than the thermal timescale. However, this is not the case in our post-collision scenario. One of the most important epochs that we must calculate accurately is the initial readjustment of the star to thermal equilibrium. By definition, this

readjustment occurs on a thermal timescale. We must therefore take timesteps which are small compared to the thermal time. Semiconvection must be modeled explicitly.

We use the approach of Langer (Langer, Sugimoto & Fricke 1983, Langer, El Eid & Fricke 1985) to add a full treatment of semiconvection to YREC. First, we determine if each shell is radiative, convective, or semiconvective according to the Ledoux and Schwarzschild criteria above. The chemical composition in each semiconvective shell is updated according to the diffusion equation

$$\frac{\partial X_i}{\partial t} = \left(\frac{\partial X_i}{\partial t} \right)_{nuc} + \frac{\partial}{\partial M_r} \left((4\pi r^2 \rho)^2 D \frac{\partial X_i}{\partial M_r} \right) \quad (4)$$

where X_i is the abundance of the i^{th} element, $\left(\frac{\partial X_i}{\partial t} \right)_{nuc}$ is the change in abundance due to nuclear burning, and D is the diffusion coefficient. This coefficient is given by

$$D = \alpha \frac{2acT^3}{9\kappa\rho^2c_p} \frac{\nabla - \nabla_{ad}}{\nabla_L - \nabla}. \quad (5)$$

where $\nabla = \frac{d \ln T}{d \ln P}$ is the actual temperature gradient in that shell and c_p is the heat capacity as calculated from the equation of state. Langer *et al.* (1985) determine the efficiency factor α to be of order 0.1, based on the expected values of $\nabla - \nabla_{ad}$ from mixing length theory, and on an analysis of the fluid dynamics by Unno (1962). Equating the eddy viscosity with the diffusion coefficient also gives $\alpha = 0.1$.

The temperature gradient also depends on the convective state of each shell of the star. This gradient, in the semiconvective region, is determined by solving $\nabla = \nabla_{rad}/(1+L^{sc}/L^{rad})$ for ∇ , where

$$L^{sc}/L^{rad} = \alpha \frac{\nabla - \nabla_{ad}}{2\nabla(\nabla_L - \nabla)} \left[(\nabla - \nabla_{ad}) - \frac{\beta(8 - 3\beta)\nabla_\mu}{32 - 24\beta - 3\beta^2} \right] \quad (6)$$

The two luminosities, L^{sc} and L^{rad} represent the amount of luminosity carried by the two energy transport mechanisms, semiconvection and radiation respectively. Here β is the ratio of gas pressure to total pressure in that shell of the star.

It can be shown that the condition for dynamical stability, $\frac{ds}{dr} > 0$, is the same as the Ledoux criterion for stability against convection for any non-rotating fluid which expands when heated (e.g. Landau & Lifshitz 1959). If a star has an entropy gradient which increases outwards, it will not be convective. This stability condition was used by LRS to determine when it was acceptable to stop the SPH simulations. Therefore, our collision products are radiative or semiconvective when they begin their thermal contraction. Our evolution calculations show that they do not develop a convective envelope until they reach the giant branch.

4.3. Results

The evolutionary tracks are plotted in figures 4 and 5. Distinguishable points are marked on each track, and the times from the collision to that point are given in table 2. We describe the details of the evolution of case A in the following paragraphs. The underlying physics of the other collisions is similar. Other specific cases will be discussed later in this section.

Position 0 is the position of the first model after the collision. Since the collision product is not in thermal equilibrium, it has a larger radius and is less concentrated than a main sequence star of the same mass. Its core is not yet hot or dense enough for any significant fusion to occur, and so the star cannot support itself against gravitational collapse on a Kelvin-Helmholtz timescale. As the star’s radius shrinks, the amount of available gravitational energy is reduced and so the luminosity also decreases. The star’s effective temperature increases, and the star moves toward the lower left corner of the HR diagram.

As the amount of gravitational energy which can be released by further contraction

decreases, the contraction slows. At the same time, the temperature of the core continues to increase so that the opacity in the core is reduced, and energy flows more rapidly. This causes the luminosity and the surface temperature of the star to increase and the track turns toward the upper left of the diagram. At the maximum luminosity of this loop, nuclear reactions begin and the gravitational contraction slows. When the star's luminosity is supplied by nuclear reactions alone, the star has reached the main sequence. The thermal relaxation phase of evolution of these collision products occurs on a global thermal timescale, $t_{th} = \frac{GM^2}{2RL}$, where M is the mass of the star, and R and L are the radius and luminosity at the start of the collapse phase.

The equivalent of the zero age main sequence is at position 1, and the turnoff, or terminal age main sequence, is position 2. Between positions 1 and 2, the star is burning hydrogen to helium in its core and is in both hydrostatic and thermal equilibrium. At position 2, the central hydrogen abundance has dropped below $X = 0.001$. Between position 2 and 3, the star is on the subgiant branch, where the energy source for the star is gravitational contraction of the core and a small hydrogen burning shell. Position 3 is the base of the giant branch, where the track turns and begins its ascent up the giant branch. Case G shows a hook in its main sequence evolution since this star has a discontinuity in the hydrogen abundance of the star created by the collision. It also develops a very small convective core about 5000 years after the collision which lasts for its entire main sequence lifetime. When the convective core moves outwards during the main sequence evolution and reaches this discontinuity, a large amount of new hydrogen is mixed into the core, so the star turns back, away from the subgiant branch and towards the main sequence briefly. However, that new fuel is quickly consumed and the star must end its main sequence life.

Case J shows an interesting kink in its track at the beginning of its evolution. Instead of collapsing immediately, the star increases in luminosity for about 1200 years, and then

collapses. This is caused by the large hump in luminosity at $m/M_* \sim 0.9$, which radiates outwards and leaves the star. This hump is created when the outer few percent of the star, which was thrown off to large distances by the collision, rains back down on the collision product and converts its gravitational energy to thermal energy when it hits the surface. After that energy has been radiated away, the star can collapse and become fainter, in the same way as the other stars. The other cases do not show this particular feature since the initial outermost luminosity is the maximum and so the star can only become fainter. Despite the large initial luminosities in the outer regions of these collision products, the structure of their outer 20% by mass is so rarefied that the luminosity can be carried by radiative transport. Therefore, none of the cases we studied developed convective envelopes during the thermal collapse phase.

Figure 6 shows the tracks from the SPH models (solid line), along with evolutionary tracks for normal stars (dotted line) and fully mixed stars (dashed line) with the same masses as our collision products. The normal tracks show the expected evolution for an initially chemically homogeneous star with a normal composition for a globular cluster ($Z = 0.001, Y = 0.25$). The fully mixed tracks also show the expected evolution for chemically homogeneous stars with a composition given for a star with the same total helium mass as the collision product.

The SPH models are brighter than the normal stars, and with a significant main sequence are hotter as well. The increased helium content of the collision product, especially the higher mass stars, has affected the opacities and the nuclear reaction rates in the stellar core. A higher helium content reduces the opacity in the core, making the star brighter. Also, this increase in luminosity coming from the core heats up the star. Case A shows a star which has depleted almost all of its hydrogen fuel, and so starts its ‘main sequence’ life well up the hydrogen exhaustion phase, never truly living on the main sequence. If most of

the massive blue stragglers evolve with very short lifetimes, their birthrates must be very large to account for their observed numbers.

The fully mixed tracks are significantly different from those of the collision products, as expected. Since the mixed stars have more helium in their envelopes, their tracks are brighter and hotter on the main sequence than the collision tracks. They also live on the main sequence for longer since these stars have more hydrogen mixed into their interiors. The ages for the normal and fully mixed tracks are given in table 2. The thermal timescale given in table 2 is the global thermal timescale at the zero-age main sequence, and represents an order of magnitude estimate for the pre-main sequence lifetime of these stars.

The effects of collisional history are demonstrated in the large differences in the tracks of case G and case J. These two stars have similar masses, (1.133 and 1.142 M_{\odot} respectively) but their evolution differs greatly due to their very different initial composition and stellar structure. Case G is a head-on collision between a turnoff mass star and a star with half this mass. Since the lower mass star begins with a lower entropy than the higher mass star, the lower mass star essentially sinks to the center of the collision product, creating a near-discontinuity in the composition and temperature profiles. These anomalous initial profiles cause the star to live on the main sequence longer than case J, which begins its life with a core only slightly depleted in hydrogen. Case G is hotter and brighter than case J on the main sequence because case G has a denser core and therefore burns its fuel more quickly. Since its luminosity is increased while its radius has remained the same, its effective temperature also increases. The remnant from case J, a head-on collision between two $0.6M_{\odot}$ stars, behaves much more like a normal star of the appropriate mass than the case G remnant since the initial temperature and composition profiles in case J mimic those of the parent stars. The increased helium content of the core of case J reduces its lifetime on the main sequence.

The four other head-on collision products which we have evolved show similar characteristics to the three discussed above. Cases M and U are another pair of collision products with similar masses but different collision histories. Case M is the product of a collision between a $0.6M_{\odot}$ star and a $0.4M_{\odot}$ star, resulting in a product with a total mass of $0.946M_{\odot}$. Case U is the remnant of a collision between a turnoff mass star ($0.8M_{\odot}$) and a very low mass star ($0.16M_{\odot}$). Again, the collision product with the larger mass ratio (case U) is hotter and brighter. The differences between cases U and M are less than those between cases G and J since the parent stars of the lower mass pair (U and M) had created less helium in their pre-collision lifetime.

Case P is not really a blue straggler, even though it is a collision product. This star is the product of a collision between two $0.4M_{\odot}$ stars, and so it has a mass slightly less than the turnoff mass of $0.8M_{\odot}$. The parent stars of this merger remnant have evolved through only a small fraction of their main sequence lifetime and so have a large amount of their hydrogen fuel left to burn. For these two reasons, the case P star evolves on a normal track for a turnoff mass star, and will be hidden among the normal main sequence stars in a globular cluster.

The track for case D lies between those for case A and case G. This is expected since case D is the product of a collision between a $0.8M_{\odot}$ star and a $0.6M_{\odot}$ star. The track shows the same sort of initial increase in luminosity as case J, a significant but fairly short-lived main sequence, and the expected evolution through the subgiant branch to the giant branch.

5. Summary and Discussion

5.1. Comparison with Pre-Main Sequence Stars

Leonard and Livio (1995) proposed that the products of stellar collisions would be similar to pre-main sequence stars in their structure and evolution. They suggested that these stars gain a large amount of thermal energy in the collision, and so they expand. The swollen objects resemble pre-main sequence stars in that they are not in thermal equilibrium, do not have sufficient temperature to start hydrogen burning, and will therefore release gravitational energy as they contract to thermal equilibrium and the main sequence on a thermal timescale.

While the collision products are indeed far from of thermal equilibrium, they have some significant differences from pre-main sequence stars. These differences all stem from the inhomogeneity of parent stars of the collision products, unlike the parent gas of normal pre-main sequence stars. Since the parent stars are evolved, they have regions with non-zero chemical composition and specific entropy gradients. This is especially true for the stars closest to the turnoff, and less true for lower mass stars, which have lived only a small fraction of their main sequence lifetimes. Also, the specific entropy of the fluid differs between stars of different masses. Therefore, if a collision occurs between two evolved stars of high mass, or between two stars of different masses, the parent gas of the collision product will not have a homogeneous entropy content. This inhomogeneity of the entropy of the parent gas, plus the shock-heating which occurred during the collisions, results in an entropy gradient in the collision product. The condition for dynamical stability is that the entropy gradient increases outwards, and so the collision product will continue to have fluid motions on a dynamic timescale until this condition is met. LRS’s calculations show that is condition is satisfied quickly for most of the star, usually on the order of a day.

5.2. Mixing

In this section, we will concentrate on an analysis of mixing in case A, the collision between two turnoff mass stars. The mixing of this collision product is most interesting, since it has the largest semiconvective region of the seven cases presented in this paper. The other six cases have chemical composition profiles which are less steep than that of case A, and smaller luminosities in the interior of the star. These two factors cause the stars to be more radiative than case A.

Figure 7 shows the interior structure of case A as a function of time from 100 years after the collision to the main sequence. The light grey region is semiconvective, the dark grey region is convective, and the white region is radiative. Very little of this star is convective at any time prior to the main sequence. Never does any helium get mixed into the outer regions of the star, and only the inner $m/M \sim 0.1$ even becomes largely convective. Small short-lived convective regions do appear sporadically throughout the star, but these are not significant in mixing most of the star. This can be seen most clearly in figure 8, which shows helium profiles of the star at 6 times during the initial thermal relaxation phase.

The core of the collision product is initially semiconvective because of the interplay between the luminosity at each shell in the star and the chemical composition profile. The initial luminosity profile of case A has a ‘hump’ in luminosity in the inner $\sim 25\%$ of the star. Normally, a large luminosity would cause the region to be convective, since convective energy transport is more efficient than radiation. However, this star also has a strong gradient in mean molecular weight in the same region as the luminosity excess, and so the region is only semiconvective, not convective. As the star begins to settle down to thermal equilibrium, this luminosity moves outwards in the star, and the luminosity profile begins to flatten out. The large luminosity region leaves the innermost part of the star first, and so the center of the star becomes radiative before the rest of the star. The outer boundary

of the semiconvective region moves outwards as the increased luminosity moves outwards and causes regions of the star at higher mass fractions to become more semiconvective. The chemical profile does not become flat until a mass fraction of ~ 0.5 , so the mean molecular weight gradient continues to stabilize the star.

If the luminosity excess were to move coherently out of the star, we would expect to see a region of the same width move from the center of the star to the edge in one thermal time. This region would be semiconvective where the mean molecular weight gradient is large enough to stabilize the region against convection, and convective where the gradient could not. However, the luminosity hump not only moves outwards, but also dissipates and heats the star slightly. Therefore, the excess in luminosity above that which can be carried by radiation gets smaller as the star evolves. This means that the semiconvective regions shrinks as it moves outwards, and by $t = 10^5$ years, radiative energy transport alone is sufficient to carry away the remaining energy. The star becomes completely radiative at this time.

The grey cross-hatched region near $t = 10^5$ years is a region in which small regions of a few mass shells each are alternatingly convective and semiconvective. This is an extreme version of the effect seen elsewhere in the star, where small convective regions are interspersed with semiconvective regions. Semiconvection is more efficient at mixing in regions of the star where the diffusion coefficient (Eq. 5) is large. Therefore, the mean molecular weight gradient is reduced more quickly in some regions than others. A reduced gradient causes more mixing, since a smaller ∇_μ means a smaller value of ∇_L and therefore a larger diffusion coefficient. Eventually the gradient of mean molecular weight becomes zero and convection begins. Therefore, regions which have more efficient semiconvection will become convective sooner. This phenomenon is discussed in more detail by Langer *et al.* (1985). In the grey cross-hatched region, the temperature gradient is very slightly

larger than the adiabatic temperature gradient (so the region is only barely semiconvective) and the efficient semiconvective regions have reduced their mean molecular weight gradient very close to zero. The distinction between radiative, convective and semiconvective in this region is becoming unclear. Eventually, however, the luminosity excess finally leaves the star, and the entire star becomes radiative. The compositional effects of this merging of convective state can be seen in figure 7.

Towards the end of the thermal collapse phase, the star develops a small central convective zone. Stars with masses more than about a solar mass have convective cores when on the main sequence, and this collision product is behaving in accordance with standard stellar evolution theory.

None of the collision products modeled here, including case A, mix significant amounts of hydrogen into their cores or helium into their envelopes. The stars do not become largely convective for two reasons. The first is the influence of the gradients in mean molecular weight, which stabilize the fluid against convection but allow semiconvection. This semiconvection reduces the mean molecular weight gradient but is too slow to mix the region completely. The second reason that these collision products do not become convective is that the large luminosities which are present in the outer regions of the star at the end of the collision escape from the star in a few thousand years since the thermal timescale in these regions is so small. Therefore, there is little convection occurring in these stars, and they do not mix.

While convection must be treated carefully, the general conclusions presented here do not depend strongly on the inclusion and details of semiconvection. Since the outer 50% or more of the case A product is radiative at any given time during the initial thermal relaxation phase (see Figure 7), this star will never completely mix. The details of the treatment of semiconvection will determine how much mixing occurs in the core of this

star, which in turn will determine the main sequence lifetime of this collision product. If semiconvection is neglected entirely, the inner 1/3 of the star will be convective and mix immediately. Under this treatment of convection, the collision product will have a central helium abundance of $Y = 0.70$. Since the star has used up most of its core hydrogen, its main sequence lifetime will still be short compared to a normal star of the same mass. Therefore, we can safely conclude that this collision product will not mix fully during its thermal relaxation phase, and that little hydrogen will be mixed into the core, resulting in a short main sequence lifetime.

5.3. Comparison with Previous Evolutionary Calculations

Bailyn and Pinsonneault (1995) showed that the luminosity function of blue stragglers in the globular cluster 47 Tuc matched the predicted luminosity function for single-star collisions. However, their evolutionary tracks were based on the assumption that a blue straggler created by a collision between two stars was fully mixed. Both the SPH calculations and the evolutionary tracks presented here bring this assumption into question. The SPH calculations show that the collision itself does not induce a significant amount of mixing. The evolution calculations of head-on collision products show that convection does not play a significant role in mixing the star during the initial thermal relaxation phase. Therefore, the blue stragglers in 47 Tuc must have been mixed by some process we have not considered (for example, rotational mixing). Alternatively, the total mass of the brightest blue stragglers could be greater than twice the turnoff mass. This might be true if triple collisions (mediated by binary- single star or binary-binary interactions) contribute significantly to the blue straggler birth rate.

Two groups have recently used a portion of the SPH results from stellar collision calculations to approximate the evolution of blue stragglers. Sills, Bailyn & Demarque

(1995) used the SPH chemical profile of a collision between two turnoff mass stars and imposed that profile on an otherwise normal stellar model. Sandquist, Bolte & Hernquist (1996) also imposed a chemical profile on a normal stellar model. They then went one step further than Sills *et al.*: following the suggestion of Leonard & Livio (1995), they arbitrarily added energy until the star was on the Hayashi track and evolved the star from that point. The resulting evolutionary tracks of these two groups are generally similar, with one major difference. The track calculated by Sandquist *et al.* for the equivalent of case A has an obvious main sequence, since the inner $\sim 0.2M_{\odot}$ of the star became convective and mixed hydrogen into the core. Sills *et al.* began the evolution on the ‘main sequence’, and since their starting model had depleted its core hydrogen, it evolves immediately to the subgiant branch.

These two tracks can be compared to the equivalent track in this paper, that of case A. In general, all three tracks occupy a similar place in the HR diagram. However, the track presented in this paper shows that Sills *et al.* underestimated and Sandquist *et al.* overestimated the amount of mixing which occurs during the thermal relaxation phase immediately after the collision. The amount of hydrogen which is mixed into the core of the star affects both the length of the main sequence in the HR diagram and the time spent as a blue straggler.

Sandquist *et al.* did not evolve the end-product of their SPH collision calculations directly, as we have done. For this reason, they did not discover that, contrary to the assumption of Leonard & Livio (1995), the star never ends up on the Hayashi track. Sandquist *et al.* state that they believe the evolution between the end of the SPH simulation and the pre-main sequence is unimportant, and they neglect all effects which occur on thermal relaxation scales or shorter. However, we have shown that the evolution during the initial thermal relaxation phase is quite important in determining the structure of the star

on the main sequence. These blue stragglers never develop a surface convection zone, and do not spend any time on the Hayashi track. Therefore, they do not mix significantly.

5.4. Physical Reliability of the Collision Models

The evolutionary tracks we have presented here depend on the assumptions made in the SPH simulations, in the evolution calculations and in the transformation process between the two kinds of codes. Most of these assumptions and their effect on the evolutionary tracks have been discussed elsewhere in this paper. There are two points, however, which have not yet been addressed.

Given the importance of the entropy profiles of the merger remnants, one might worry that the SPH artificial viscosity might be significant for the subsequent stellar evolution. However, substantial changes in the artificial viscosity parameters only weakly affect the resulting entropy and chemical composition profiles (see §4.2 of LRS). Indeed, due to the typically low velocity dispersions in globular clusters, the stellar collisions we consider are rather weak and shocks are not the dominant effect. Nevertheless, our SPH code has been well tested in the presence of shocks (eg. Rasio & Shapiro 1991). We have tested its treatment of one-dimensional shocks for Mach numbers $\mathcal{M} \sim$ a few, and for the artificial viscosity parameters used in LRS: we find that a shocked region typically has a final value of $P/\rho^{5/3}$ which is only marginally ($\sim 2\%$) larger than in accurate, high resolution simulations done with a one-dimensional SPH code. Although artificial viscosity can spuriously transport angular momentum and produce entropy in differentially rotating stars where there is shear but no shocks, that is of no concern here since we treat only head-on collisions.

One crucial assumption in the SPH simulation is the use of polytropes as parent stars

in the collision. Polytropes with indices $n = 1.5$ or $n = 3$ (as used in LRS) are reasonable approximations to zero age main sequence stars, but it is not clear that they are sufficient to model evolved stars. In particular, the increase in central mean molecular weight due to nuclear burning causes a significant decrease in central entropy. Since the structure of the collision product is determined by its entropy profile, this change in entropy is important (Sills & Lombardi 1997). Therefore, the tracks presented here may not have initial conditions appropriate for collisions between significantly evolved stars.

5.5. Future Work

Here we have evolved only non-rotating, head-on collision products. However, grazing incidence collisions are more likely to occur in globular clusters. LRS also calculated collisions with non-zero impact parameters, resulting in rapidly rotating collision products. Due to centrifugal support, rotating stars have lower central temperatures and densities than their non-rotating counterparts. Consequently, they will evolve more slowly and spend more time on the main sequence. Another crucial effect rapid rotation will have on the evolution of a star is mixing, caused by meridional circulation. The global timescale for meridional circulation is (Tassoul 1978) $\tau_c = \tau_{therm}/\chi$, the thermal timescale divided by the ratio of the centrifugal to gravitational acceleration. For the collision products calculated by LRS (see their table 3), the values of χ are typically on the order of 20-70% in the equatorial plane, suggesting that a significant fraction of the star could be mixed by rotation before it reaches the main sequence. Our fully mixed models presented in this paper represent the most extreme case of mixing possible, from rotation or other sources, and so provide a limiting case of the evolution of the rotating collision products. The differences between a mixed star and an unmixed star in temperature, luminosity and lifetime are significant, and so future evolutionary models of stellar collision products will need to include the effects of

rotation.

Although grazing incidence collision products are rapidly rotating at the end of the SPH simulations, rapid rotation rates are not seen in blue stragglers in globular clusters and old open clusters (Mathys 1991). Therefore, if blue stragglers are indeed created in stellar collisions, some mechanism must spin the stars down between the collision and their appearance on the main sequence. Recent results have shown that classical T Tauri stars, young stars with circumstellar disks of masses down to about $0.01 M_{\odot}$, are all rotating with periods of about 8.5 days (Edwards *et al.* 1993). One current scenario (Königl 1991) suggests that magnetic coupling locks the disk to the star, transferring angular momentum to the disk and forcing these stars to rotate with relatively long periods. If stellar collision products have both magnetic fields and disks created during the encounter, they could be slowed down by the same mechanism as pre-main sequence stars. Since low mass stars typically have magnetic fields, their collision products should also. The collision also throws off a few percent of the stellar material, which can amount to as much as $0.1 M_{\odot}$. If even a tenth of this material were to remain in orbit around the new star, this disk could slow the star’s rotation enough to match the observations. These speculations will need to be confirmed with further calculations of the pre-main sequence evolution of blue stragglers.

Light elements, such as lithium, beryllium and boron, are burned at low temperatures and are therefore excellent tracers of mixing and surface convection in stars. In particular, it is possible that if blue stragglers were created from the collision of two stars which did not have significant surface convection zones during their first foray on the main sequence (such as two turnoff mass stars), lithium could still be preserved on its surface. Since we predict that the collision products presented in this paper do not mix and do not develop surface convection zones, we could also predict that these products should have observable lithium. Lithium will not be destroyed in the collision since the collision timescale is too

short to burn any significant amount of lithium, even if the temperature gets hot enough. Detailed models of the light element abundances, including the effects of rotational mixing would be needed to analyze observed abundances quantitatively. A second popular creation mechanism for blue stragglers is the merger of the two stars of a binary. When a binary system merges, it is expected (Webbink 1979) that the secondary star essentially pours itself on the primary. This results in a star without observable lithium, since the hotter inner regions of the secondary, where lithium has already been destroyed, presumably end up on the surface of the blue straggler. If more sophisticated models confirm that lithium is indeed present on the surfaces of collision products, we may have a tracer to distinguish between blue stragglers created by stellar collisions and those created by the merger of binary stars.

5.6. Summary

We have shown that it is possible to use the results for SPH calculations directly as starting models for stellar evolution calculations with YREC. In order to deal correctly with the problems arising from the different physical assumptions of each code, the evolution through the initial thermal relaxation must be dealt with carefully. Small timesteps must be taken, and semiconvection must be treated explicitly.

We have evolved seven representative cases of head-on stellar collisions in globular clusters and discussed three of those cases in detail. A collision between two turnoff mass stars forms the highest mass blue straggler possible in this creation mechanism. The other two cases represent typical mass blue stragglers created in very different kinds of collisions. A comparison of the latter two tracks demonstrate that collisional history is very important in determining the lifetimes and positions in the HR diagram of these stars. From the seven cases presented here, we conclude that blue stragglers which are created by

head-on collisions are not significantly mixed either during the collision or subsequently by convection.

The interesting scenario proposed by Leonard and Livio (1995), in which thermal energy deposited in the collision products leads to thorough convective mixing, is not borne out by our calculations. This poses a problem for both the low observed rotation rates of blue stragglers and for the blue stragglers in some clusters which have been identified as being fully mixed stars on the basis of their location in the HR diagram. Evolution studies including rotation may be required to resolve this problem.

We would like to thank Constantine Deliyannis, Marc Pinsonneault and Ramesh Narayan for useful discussions. This work was supported by NASA grants NAGW-2469 and NAG5-2867 at Yale University and NSF grant AST 91-19475 and NASA grant NAG5-2809 at Cornell University. CB is partially supported by a National Young Investigator grant from NSF. FAR is supported by an Alfred P. Sloan Foundation Fellowship. Hydrodynamic simulations were performed at the Cornell Theory Center, which receives major funding from the NSF and IBM Corporation, with additional support from the New York State Science and Technology Foundation and members of the Corporate Research Institute.

A. Deviations from Spherical Symmetry

Head-on collision products have spherically symmetric density and entropy profiles when the star has returned to hydrostatic equilibrium. However, this does not necessarily mean that the chemical composition is also spherically symmetric (cf. fig. 10 of LRS). Some of the SPH particles have been shock heated during the collision, and so their entropy has been increased. The particles will settle into their stable configuration, with entropy increasing outward. At the end of the SPH calculation, shock heated particles will be at

the same radius as other particles which were not shock heated, but simply started out with higher entropy. The chemical composition of these two particles is most likely not the same, and we have a spherical shell of constant entropy made up of particles with different chemical composition. Since YREC insists on spherical symmetry in all quantities, we assigned the chemical composition of each shell to be the average of the compositions of the particles in that shell. This approximation is reasonable, as can be shown by considering the stability of these different particles.

Consider a fluid element which is in mechanical equilibrium with its surroundings, but with a different mean molecular weight. The fluid element must then have a different temperature than its surroundings. In this case the differential ideal gas equation of state can be written

$$\frac{d\mu}{\mu} = \frac{dT}{T}$$

since dP and $d\rho$ are equal to zero. Therefore, the element must transfer heat to or from its surroundings. Pressure balance occurs essentially instantaneously, and the mean molecular weight of the element is unchanged, so the density must change to compensate for the change in temperature of the element. The element will now start to sink or rise, depending on the sign of the difference in density between the element and the surroundings. The element will continue to sink (for example) until it reaches a layer of the star with the same density. There it would stop, except that the mean molecular weight of this new layer is probably not that of the fluid element. If the chemical composition is different, the temperature must be different, and the process continues. Eventually, the fluid element will end up in a region with the same mean molecular weight and the slow movements will stop. The timescale over which this process operates is the local thermal timescale. The details of this process will only be important during the initial thermal relaxation phase. The effect of these oscillations will be an averaging of chemical composition as elements with the same composition move towards each other. Therefore, we feel that averaging over spherical

shells is a reasonable approximation, and will not greatly affect the calculated amount of mixing or the evolution of the star.

REFERENCES

- Alexander, D. R. & Ferguson, J. W. 1994, *ApJ*, 437, 879
- Bailyn, C. D. 1995, *ARA&A*, 33, 133
- Davies, M. B., & Benz, W. 1995, *MNRAS*, 276, 876
- Davies, M. B., Benz, W., Hills, J. G. 1994, *ApJ*, 424, 870
- Edwards, S., Strom, S. E., Hartigan, P., Strom, K. M., Hillenbrand, L. A., Herbst, W.,
Attridge, J., Merrill, K. M., Probst, R., Gatley, I. 1993, *AJ*, 106, 372
- Elson, E., Hut, P., & Inagaki, S. 1987, *ARA&A*, 25, 565
- Green, E. M., Demarque, P., & King, C. R. 1987 Revised Yale Isochrones, Yale University
Observatory
- Guenther, D. B., Demarque, P., Kim, Y.-C., & Pinsonneault, M. H., 1992 *ApJ*, 387, 372
- Hills, J. G. & Day, C. A. 1976, *Astrophysical Letters*, 17, 87
- Iglesias, C. A. & Rogers, F. J. 1996, *ApJ*, 464, 943
- Königl, A. 1991, *ApJ*, 370, L39
- Kippenhahn, R. & Weigert, A. 1994, *Stellar Structure and Evolution* (Berlin:Springer
Verlag)
- Landau, L. D., & Lifshitz, E. M. 1959, *Fluid Mechanics* (New York: Pergamon Press)
- Langer, N., El Eid, M. F., & Fricke, K. J. 1985, *A&A*, 143, 179
- Langer, N., Fricke, K. J. & Sugimoto, D. 1983, *A&A*, 126, 207
- Leonard, P. J. T. 1989, *AJ*, 98, 217
- Leonard, P. J. T. & Livio, M. 1995, *ApJ*, 447, L121
- Lombardi, J. C., Rasio, F. A., & Shapiro, S. L. 1995, *ApJ*, 445, L117

- Lombardi, J. C., Rasio, F. A., & Shapiro, S.L. 1996, ApJ, 468, 797 (LRS)
- Mathys, G. 1991, A&A, 245, 467
- McMillan, S. L. W., & Hut, P. 1996, ApJ, 467, 348
- Ouellette, J. & Pritchett, C. 1996, in ASP Conference Series # 90 The Origins, Evolution and Destinies of Binary Stars in Globular Clusters, ed. E. F. Milone, 356
- Rasio, F. A. 1991, PhD Thesis, Cornell University
- Rasio, F. A., & Shapiro, S. L. 1991, ApJ, 377, 559
- Sandquist, E., Bolte, M., & Hernquist, L. 1997, ApJ, 477, 335
- Sigurdsson, S., Phinney, E. S. 1993, ApJ, 415, 631
- Sills, A. P., Baily, C. D., & Demarque, P. 1995, ApJ, 455, L163
- Sills, A., & Lombardi, J. C. 1997 ApJ, submitted.
- Stryker, L. 1993, PASP, 105, 1080
- Tassoul, J.-L. 1978, Theory of Rotating Stars, (Princeton:Princeton Univ. Press)
- Webbink, R. F. 1979, ApJ, 227, 178
- Unno, W. 1962, PASJ, 31, 276

Fig. 1.— Profiles of luminosity L , helium abundance Y , temperature T , radius R , pressure P and density ρ versus mass fraction for the collision product of case A. This collision is a head-on collision between two $0.8M_{\odot}$ stars, resulting in a product with a total mass of $1.498M_{\odot}$. The large increase in luminosity in the outer 20% of the star is caused by the released gravitational energy of gas which was ejected from the star by the collision and then fell back onto the collision product.

Fig. 2.— Same as figure 1 for case G. This collision is a head-on collision between a $0.8M_{\odot}$ star and a $0.4M_{\odot}$ star, resulting in a product with a total mass of $1.133M_{\odot}$. Notice the discontinuity in helium abundance at a mass fraction of 0.2. Interior to this point lies the majority of the smaller parent star, which has lower entropy and so sank to the center of the collision product. The evolved core of the turnoff-mass star has been displaced by this low-entropy material and so the maximum helium abundance occurs away from the stellar core.

Fig. 3.— Same as figure 1 for case J. This collision is a head-on collision between two $0.6M_{\odot}$ stars, resulting in a product with a total mass of $1.142M_{\odot}$.

Fig. 4.— Evolutionary tracks for three head-on collisions: cases A, G and J. Each track is labeled near the main sequence. Important evolutionary stages are marked and discussed in the text.

Fig. 5.— Evolutionary tracks for four head-on collisions: cases D, M, U and P. Each track is labeled as in figure 4.

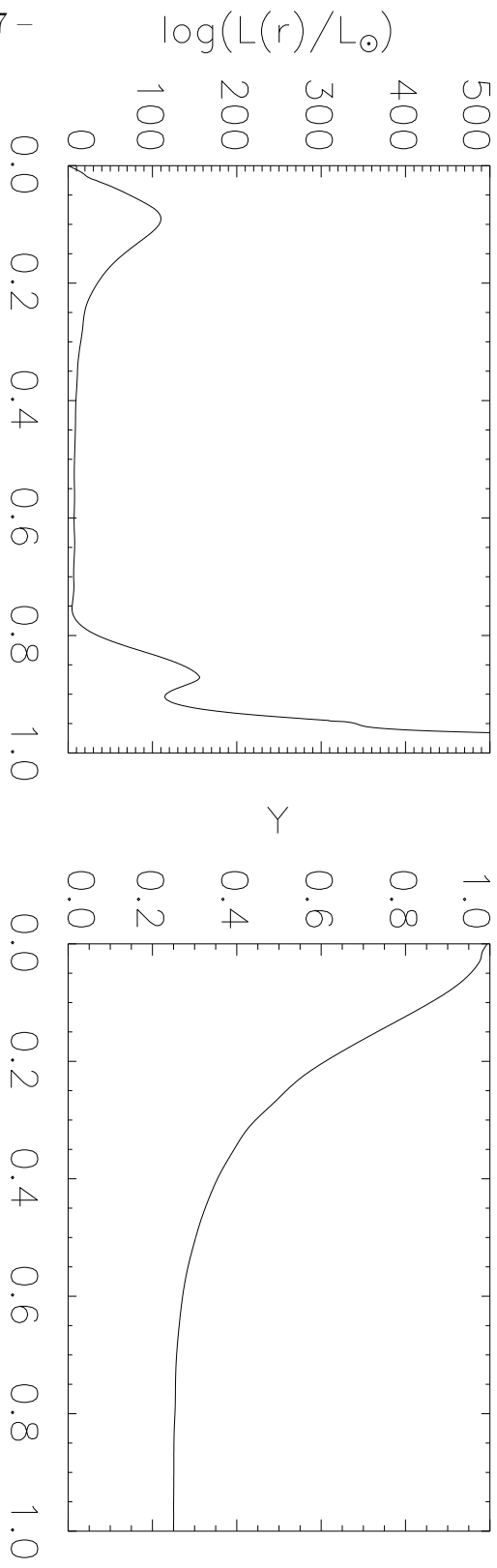
Fig. 6.— Evolutionary tracks for the collision product (solid line), a star with the same mass and the composition of a normal globular cluster star (dotted line), and a version of the collision product which was fully mixed before evolution was started (dashed line). The normal and fully mixed evolutionary tracks are shown only from the zero age main sequence

onwards. The top panel shows case A, the middle shows case G and the bottom shows case J. Notice that case J follows the evolutionary path of a normal star of the same mass but starts its main sequence evolution about half-way up the main sequence. This is expected since the star has a composition profile quite similar to the composition profile of the parent stars, which are partially evolved main sequence stars.

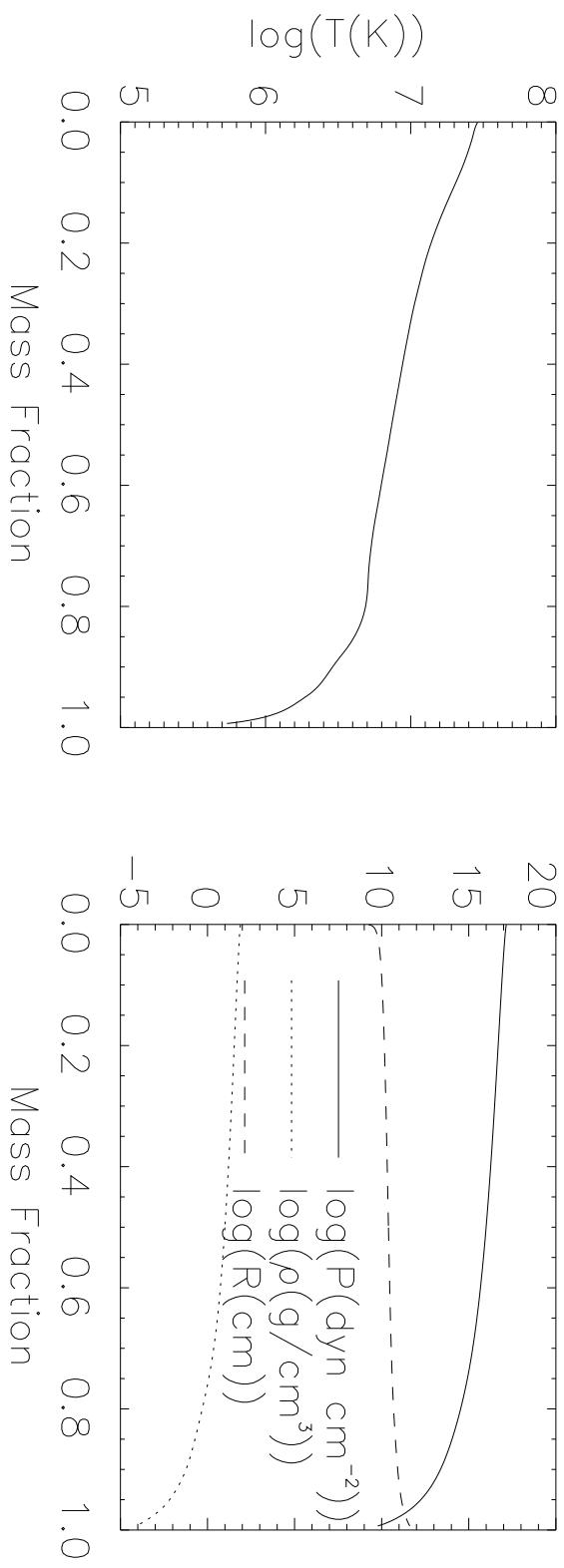
Fig. 7.— A plot of the convective state of case A as a function of time during the initial thermal relaxation stage of the star. The light grey regions are semiconvective, the dark grey regions are convective and the white regions are radiative. The cross-hatched region is a transition region between the semiconvective and radiative state. The majority of the star is always radiative. The inner third of the star develops small convective zones as semiconvection begins to level out the chemical profile. However, these convective zones never cover a significant fraction of the star.

Fig. 8.— Six profiles of helium abundance as a function of mass fraction for 6 ages during the initial thermal relaxation stage for case A. The profiles are for ages of 0, 10^2 , 10^3 , 10^4 , 10^5 and 10^6 years after the collision. Note the appearance of the fully mixed zones which correspond to the convective zones in figure 7. Also notice that the overall shape of the profile does not change significantly during this phase.

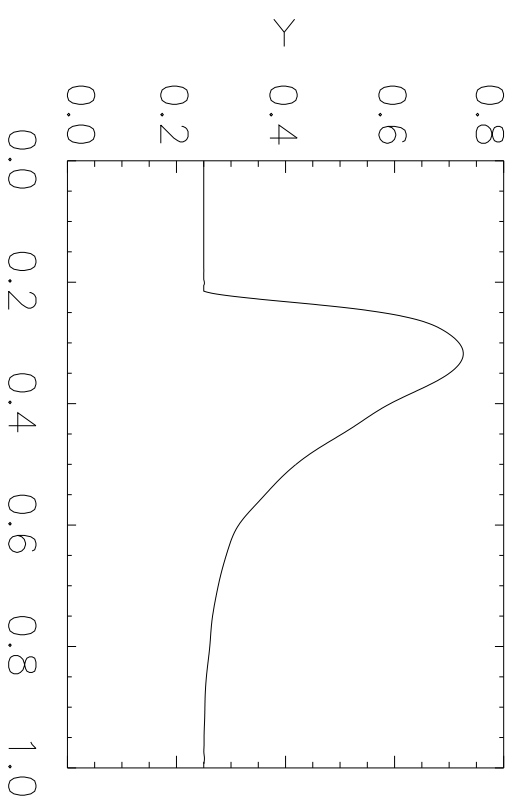
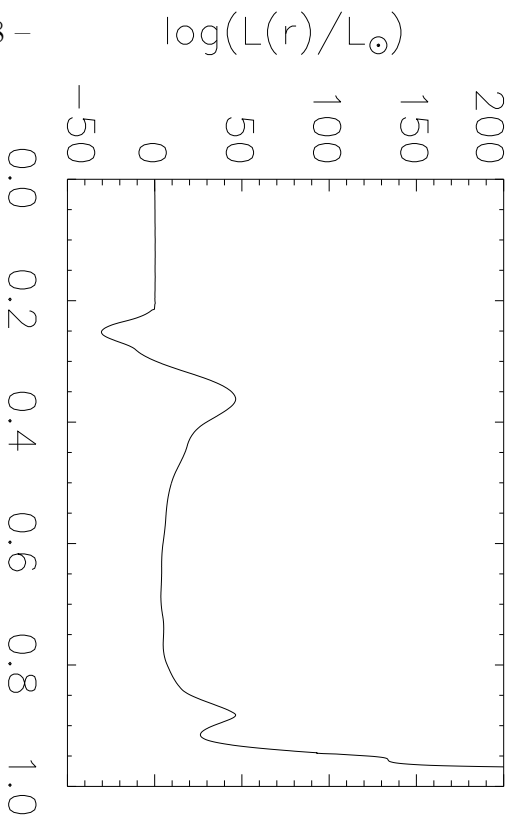
Case A: $0.8 M_{\odot} + 0.8 M_{\odot}$



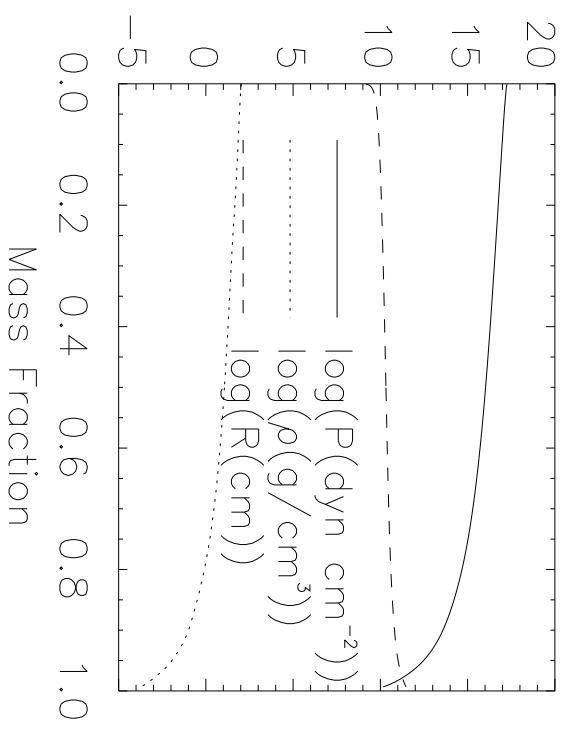
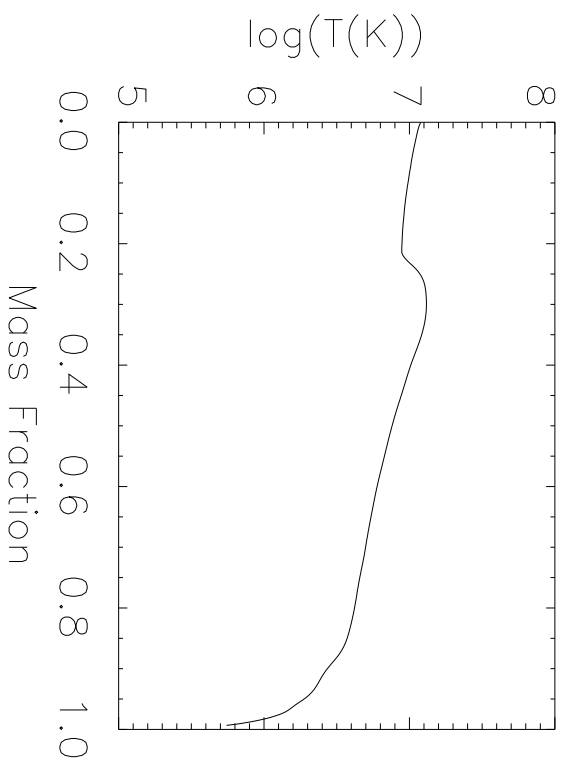
- 37 -



Case G: $0.8 M_{\odot} + 0.4 M_{\odot}$

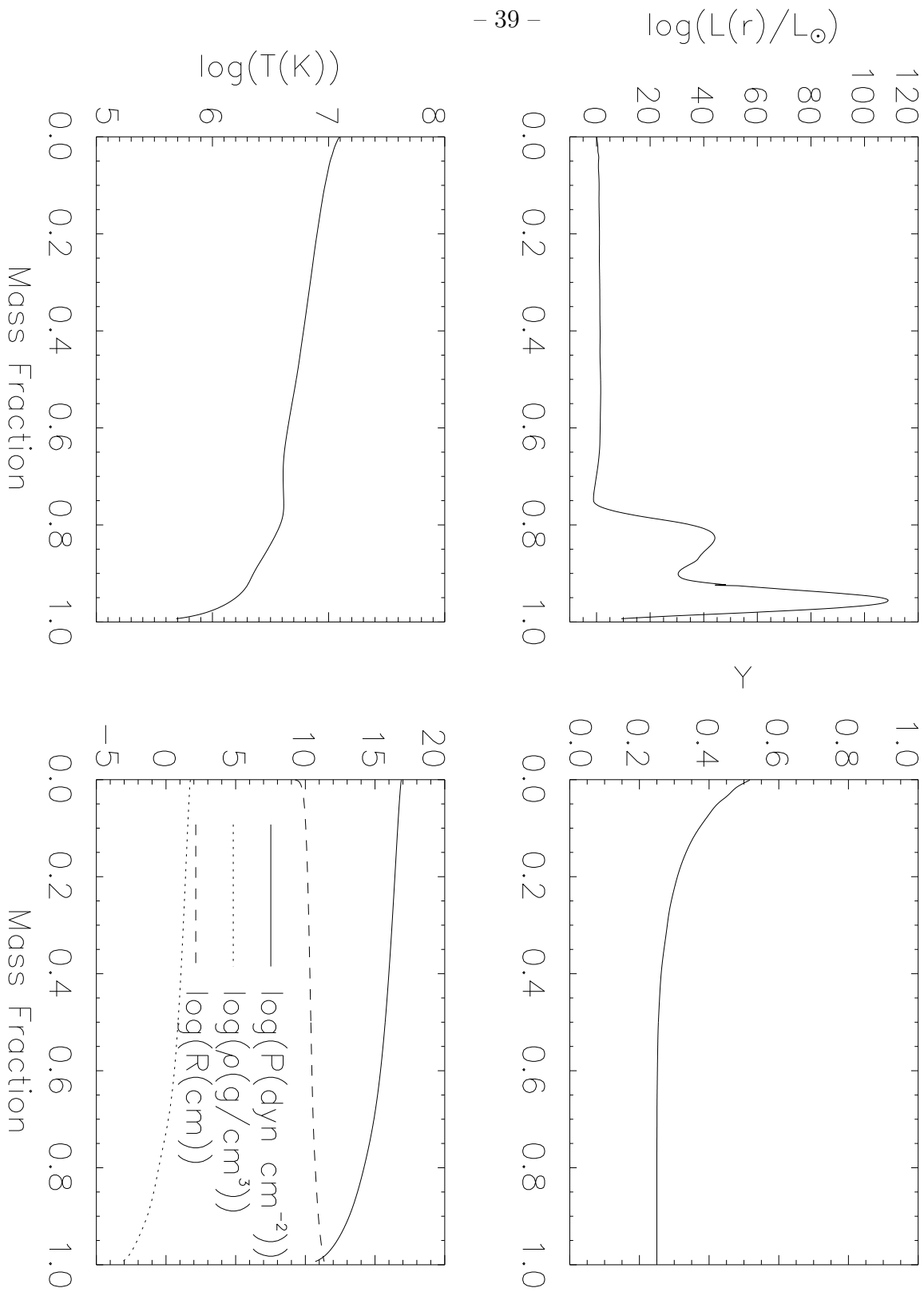


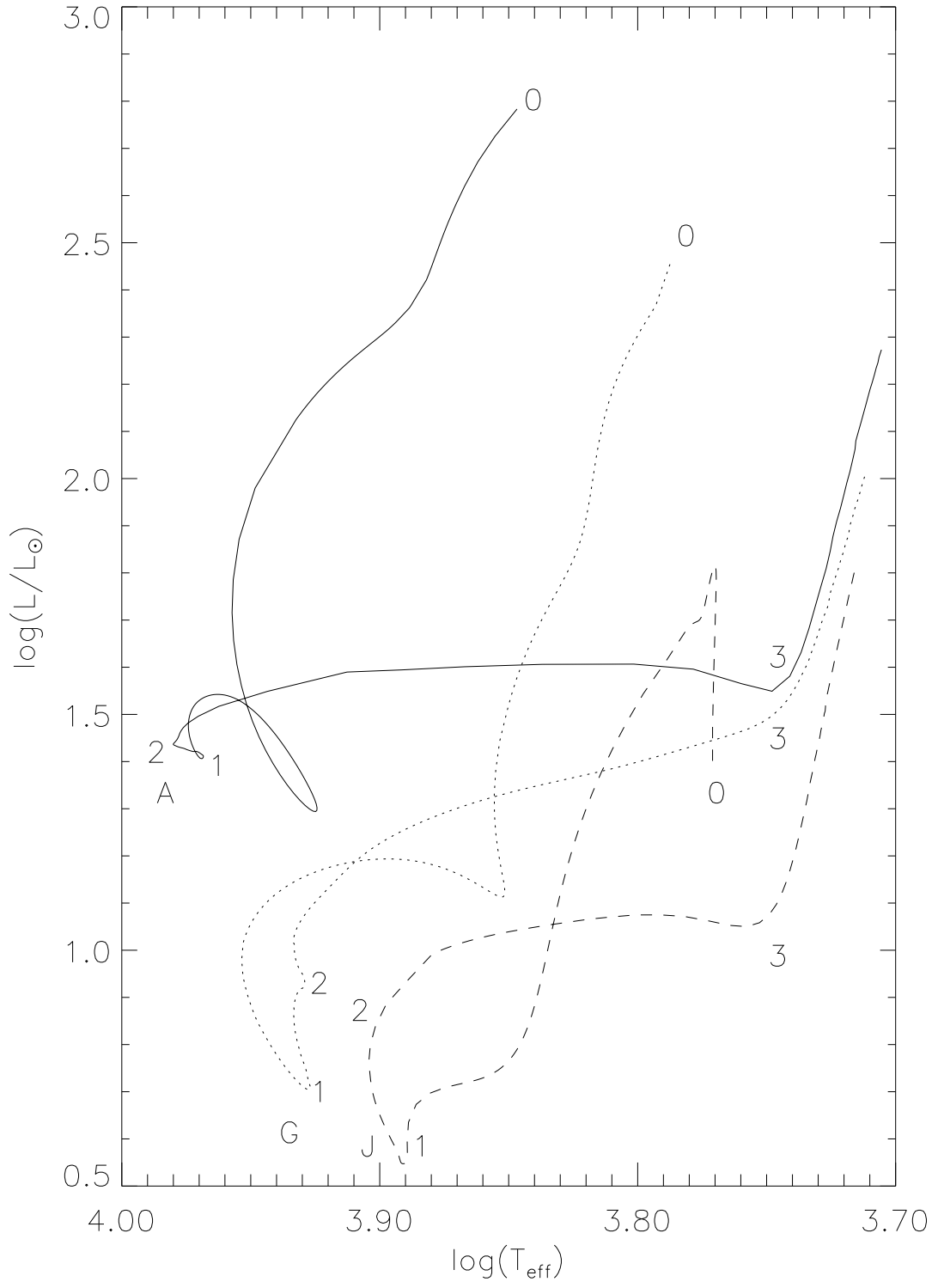
- 38 -

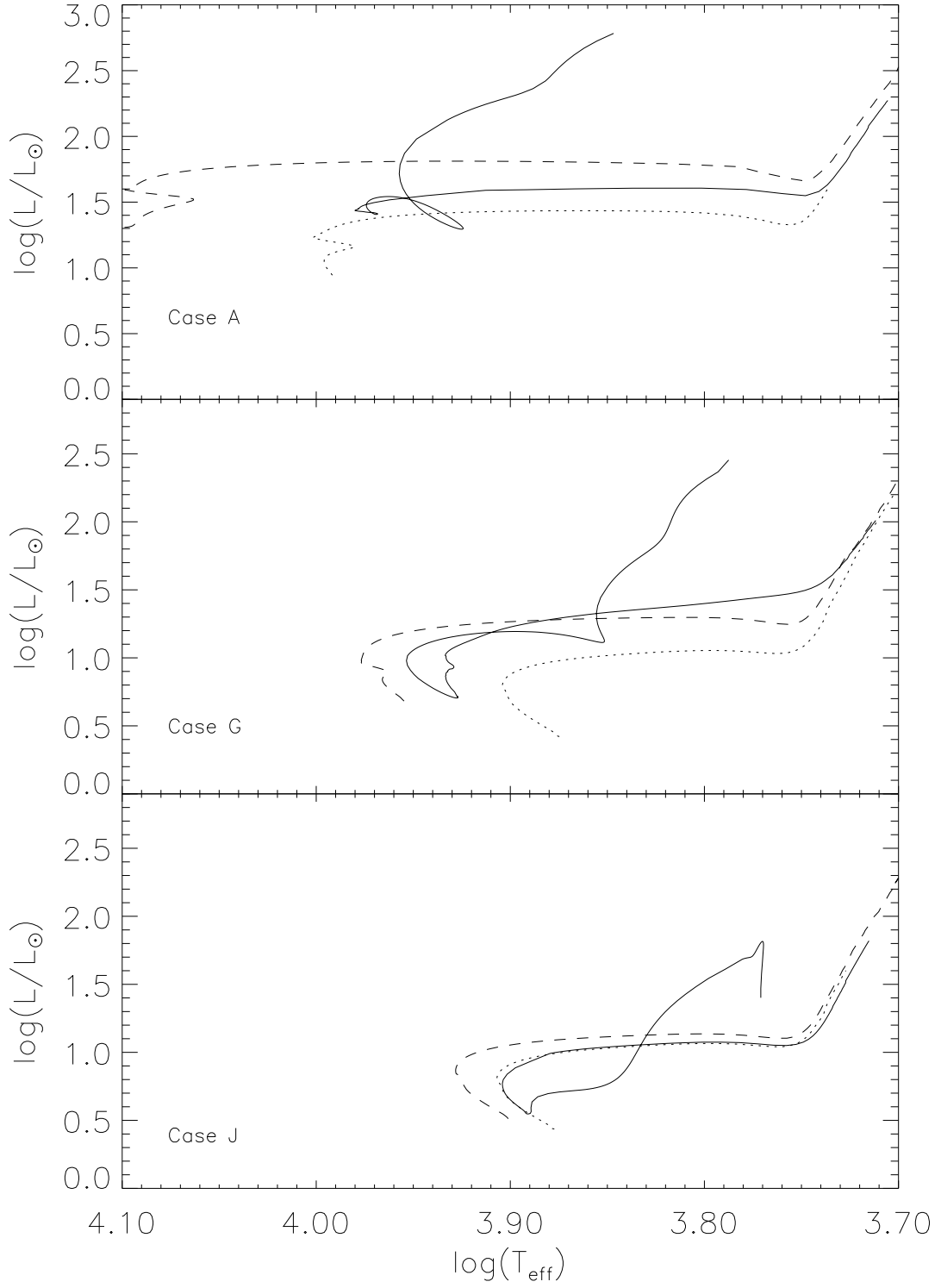


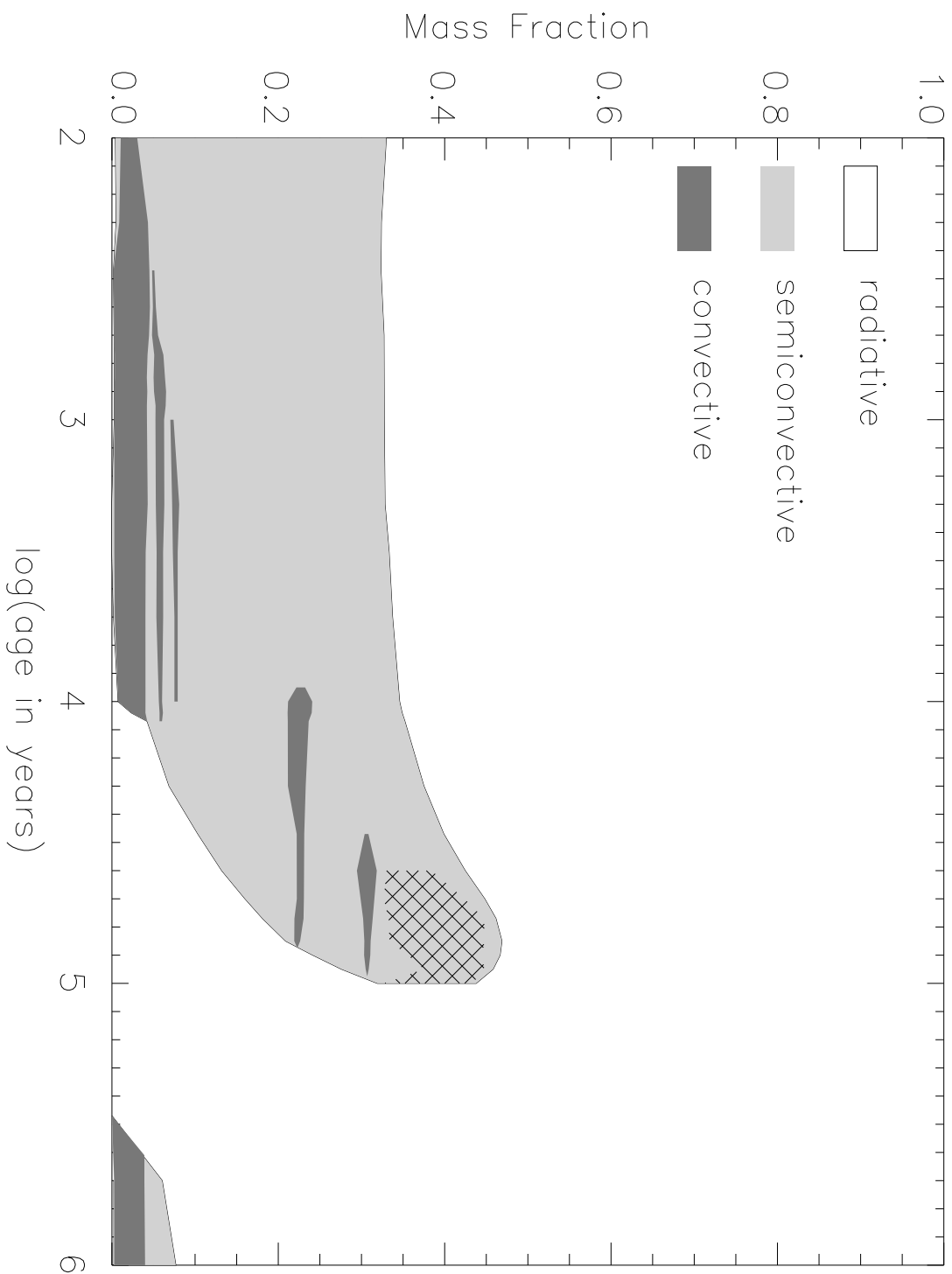
Case J: $0.6 M_{\odot} + 0.6 M_{\odot}$

- 39 -









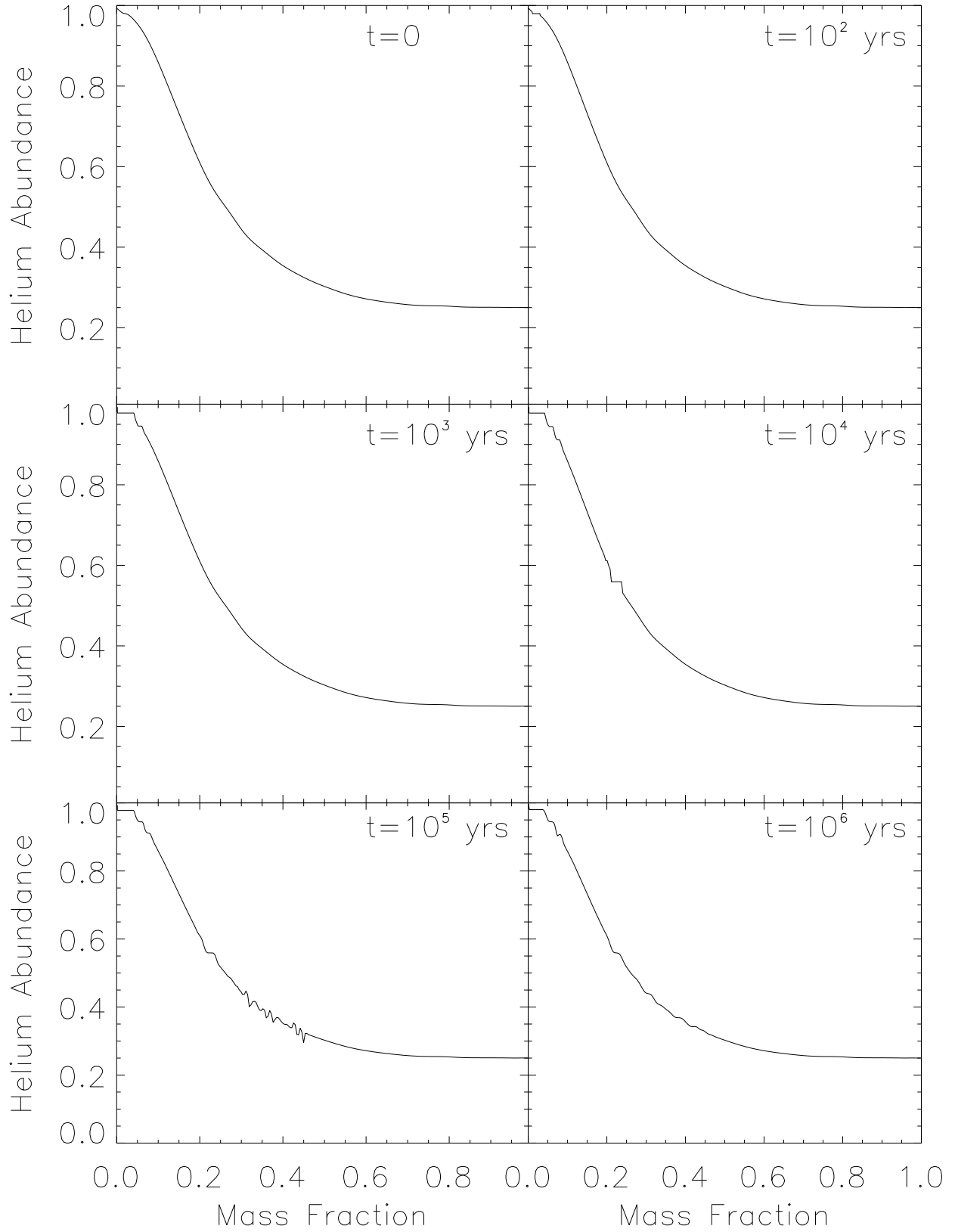


Table 1. Summary of Collisions

Case	M_1 (M_\odot)	M_2 (M_\odot)	M_{total} (M_\odot)	Helium Fraction	Global Thermal Timescale (yrs)	Local Thermal Timescale center (yrs)	Local Thermal Timescale $m/M = 0.95$ (yrs)
A	0.8	0.8	1.498	0.422	7.0×10^5	7.7×10^6	2.0×10^3
D	0.8	0.6	1.320	0.362	1.2×10^6	1.1×10^9	4.5×10^3
G	0.8	0.4	1.133	0.363	8.5×10^5	1.7×10^9	6.8×10^3
J	0.6	0.6	1.142	0.284	6.8×10^5	2.1×10^8	4.9×10^3
M	0.6	0.4	0.946	0.270	3.3×10^5	2.8×10^{10}	3.2×10^4
P	0.4	0.4	0.770	0.250	2.2×10^6	2.2×10^{10}	2.3×10^4
U	0.8	0.16	0.935	0.385	2.5×10^4	3.0×10^{10}	2.0×10^4

Table 2. Age of Star (in years) at Positions in HR Diagram

Case	(1)	(2)	(3)
	Zero Age Main Sequence	Terminal Age Main Sequence	Giant Branch
A collision	1.12×10^6	4.47×10^6	8.85×10^7
D collision	3.51×10^6	3.78×10^8	6.19×10^8
G collision	2.82×10^6	1.42×10^9	1.99×10^9
J collision	1.41×10^7	1.80×10^9	2.95×10^9
M collision	7.11×10^6	5.90×10^9	7.00×10^9
P collision	1.42×10^7	1.60×10^{10}	1.75×10^{10}
U collision	4.31×10^6	1.84×10^9	3.06×10^9
Thermal timescale			
A normal	3.86×10^6	1.24×10^9	1.58×10^9
G normal	7.85×10^6	3.38×10^9	4.13×10^9
J normal	7.63×10^6	3.28×10^9	4.02×10^9
A fully mixed	1.80×10^6	4.83×10^8	5.62×10^8
G fully mixed	4.60×10^6	1.52×10^9	2.02×10^9
J fully mixed	6.57×10^6	2.62×10^9	3.26×10^9